Supporting Information for:

Insights into the Li Diffusion Dynamics and Nanostructuring of $H_2Ti_{12}O_{25}$ to Enhance Its Li Storage Performance

Soomin Park,[†,§] *Young Geun Yoo,*[†,§] *Inho Nam,*[†] *Seongjun Bae,*[†] *Jongseok Park,*[†] *Jeong Woo Han,*[‡] *and Jongheop Yi*[*,†]

[†]World Class University (WCU) Program of Chemical Convergence for Energy & Environment, School of Chemical and Biological Engineering, Institute of Chemical Processes, Seoul National University, Seoul 151-742, Republic of Korea.

[‡]Department of Chemical Engineering, University of Seoul, Seoul 130-743, Republic of Korea.

[§]These authors (S. Park and Y. G. Yoo) contributed equally to this work.

[*]Address correspondence to jyi@snu.ac.kr.

Supporting Figures and Tables

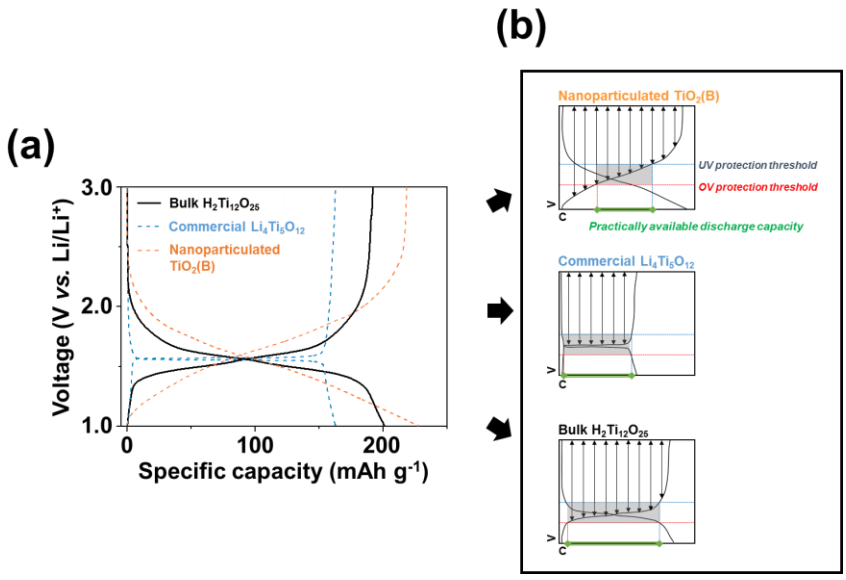

Figure S1. (a) Typical charge/discharge voltage profiles for HTO, $Li_4Ti_5O_{12}$, and TiO_2(B) obtained at 10 mA g^{-1}. The commercially available LTO sample was purchased from Posco ESM Co. Ltd. The nanoparticulated TiO_2(B) was synthesized according to a previous report.[9] Briefly, a sample of titanium foil was dissolved in an aqueous solution of H_2O_2 and NH_3, and the resultant solution was then mixed with glycolic acid. The products (a yellow gel) were sealed in a Teflon-lined stainless steel autoclave and heated at 160 ºC for 30 min. After washing and drying, nanoparticulated TiO_2(B) powders were obtained. (b) Schematic illustrations comparing the voltage profiles of 3 types of titanate-based anode materials. Practically available discharge capacity, under-voltage/over-voltage protection thresholds are denoted.

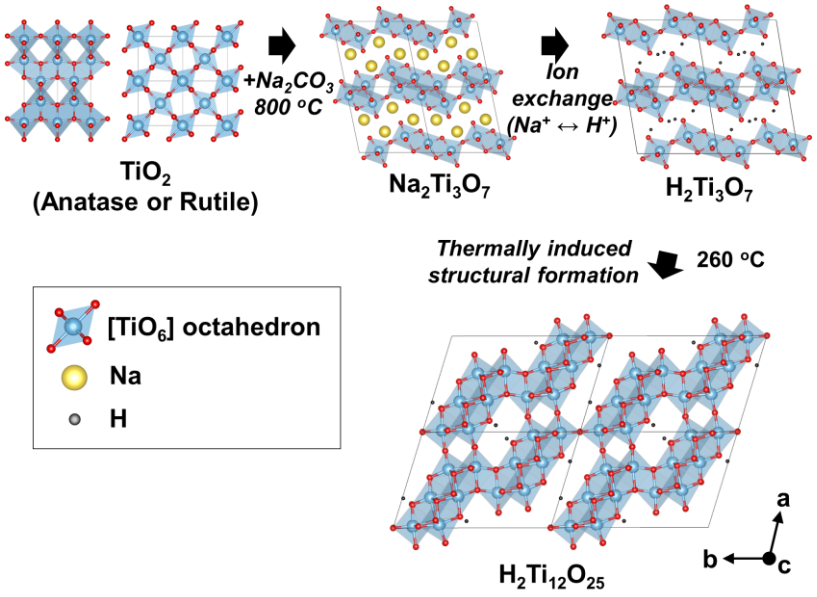

Figure S2. Synthesis of HTO crystals via a sequential process involving the recrystallization of TiO_2, ion exchange, and thermally induced dehydration/structural formation. Hexahedrons represent the boundary of a primitive unit cell. For the synthesis of HTO, $Na_2Ti_3O_7$ as a parent crystal was first prepared *via* a solid state reaction between TiO_2 and Na_2CO_3 at 800 °C.[12] The crystal structure of the starting TiO_2 is highly important and determines the shape and size of the final HTO products. In this study, we utilized three types of TiO_2 with different crystalline structures: pure anatase or rutile and an anatase/rutile-mixed phase. The produced $Na_2Ti_3O_7$ crystals can be efficiently converted to $H_2Ti_3O_7$ *via* an ion exchange step between Na^+ and H^+.[S2,S3] $H_2Ti_3O_7$ with a layered structure is rearranged to form final HTO crystals during thermally induced dehydration and condensation reactions.[11]

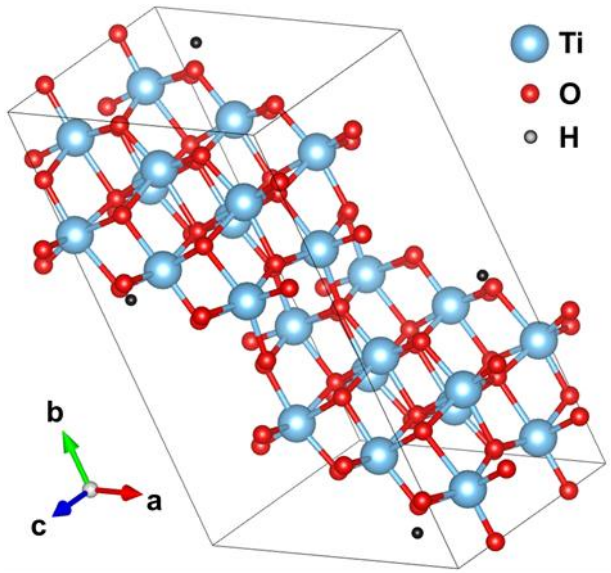

Figure S3. DFT-optimized crystal structure of $H_4Ti_{24}O_{50}$. Hexahedron represents the boundary of a primitive unit cell. The coordinates of this structure are presented below.

Coordinates of $H_4Ti_{24}O_{50}$

Unit cell (Å)

X	Y	Z
9.4775307667714586	-0.0907339953220821	-0.0050687142392930
-4.2311319016390598	14.2742692283106809	0.0013427561070414
-0.0055735329651447	-0.0025817149010813	7.7947458599171524

Atom	Cartesian coordinates		
	X	Y	Z
Ti	8.752673452	1.714004186	2.000160169
Ti	8.841069336	1.731665574	5.839629612
Ti	5.703452977	2.505454062	1.976972628

Ti	5.653498070	2.604665863	5.861759004
Ti	2.661355185	3.380330433	1.991120013
Ti	2.668621196	3.440557588	5.846370179
Ti	-3.740363928	12.498154468	1.955294140
Ti	-3.651969067	12.515813523	5.794763583
Ti	-0.552792659	11.625155345	1.933165329
Ti	-0.602748676	11.724362481	5.817952286
Ti	2.432084190	10.789262771	1.948556825
Ti	2.439350047	10.849486744	5.803807223
Ti	1.694422487	5.743501735	0.024538634
Ti	1.717368407	5.750441766	3.903423059
Ti	-2.810521754	10.203449579	7.768334101
Ti	-2.761153530	10.096517617	3.872819175
Ti	0.333999673	9.275942536	7.743668866
Ti	0.209213706	9.209569344	3.889083325
Ti	3.406282158	8.486317351	7.770389537
Ti	3.383337086	8.479377320	3.891504410
Ti	7.911226639	4.026369084	0.026591183
Ti	7.861858379	4.133301046	3.922106436
Ti	4.766705103	4.953876126	0.051258302
Ti	4.891491223	5.020249743	3.905843679
O	1.065944218	2.563339218	1.975780670
O	1.088258824	2.573800359	5.875949133
O	1.907503893	5.366039214	1.955630053
O	1.926416217	5.369771544	5.876095950

O	3.912773290	1.900855395	1.957109373
O	3.947410593	1.964857175	5.880897234
O	4.695406096	4.506336384	1.962374105
O	4.717035740	4.513028480	5.884227096
O	6.865588285	1.108993522	1.958591480
O	6.812322697	1.028093263	5.889224445
O	7.640722477	3.655012062	1.969925882
O	7.611263131	3.608266332	5.876672532
O	4.012447011	11.656018092	1.918974619
O	4.034759325	11.666480718	5.819143082
O	3.174287322	8.860048391	1.918830589
O	3.193202427	8.863779024	5.839296486
O	1.153295055	12.264962336	1.914028493
O	1.187930858	12.328963480	5.837816238
O	0.383669538	9.716793151	1.910699676
O	0.405297790	9.723480582	5.832552667
O	-1.711617107	13.201726462	1.905695474
O	-1.764883804	13.120824295	5.836328555
O	-2.510557074	10.621555300	1.918252614
O	-2.540018400	10.574804056	5.824999496
O	-3.549215455	12.005780462	7.777852573
O	-3.509141814	12.000482831	3.863479345
O	-1.514058236	8.498892538	7.723199991
O	-1.505771100	8.585676477	3.891174769
O	-0.095633397	5.146202727	0.005352714

O	-0.059273892	5.118564480	3.939219430
O	-0.762237266	11.047450097	7.776323076
O	-0.728675951	11.101931217	3.870522605
O	1.368148494	7.674915236	7.768184961
O	1.387966377	7.671697331	3.888465161
O	2.922765592	3.981580208	0.022602623
O	2.899697570	3.975760859	3.919272777
O	8.649920101	2.224038837	0.017072195
O	8.609846410	2.229336256	3.931446034
O	6.614762877	5.730926547	0.071731042
O	6.606476250	5.644143033	3.903754326
O	5.196337631	9.083616783	7.789574228
O	5.159978696	9.111255032	3.855703161
O	5.862942348	3.182369414	0.018602834
O	5.829381164	3.127887869	3.924403005
O	3.732556279	6.554903425	0.026744973
O	3.712739398	6.558121755	3.906463005
O	2.177939054	10.248238878	7.772324639
O	2.201007640	10.254058227	3.875655156
O	-4.350533925	14.229413787	1.988443857
O	9.451239303	0.000405010	5.806481056
H	6.840400855	6.434844015	0.711136052
H	-1.739694960	7.794974223	7.083790661
H	-1.422022179	14.141795579	1.911731227
H	6.522727061	0.088023748	5.883176148

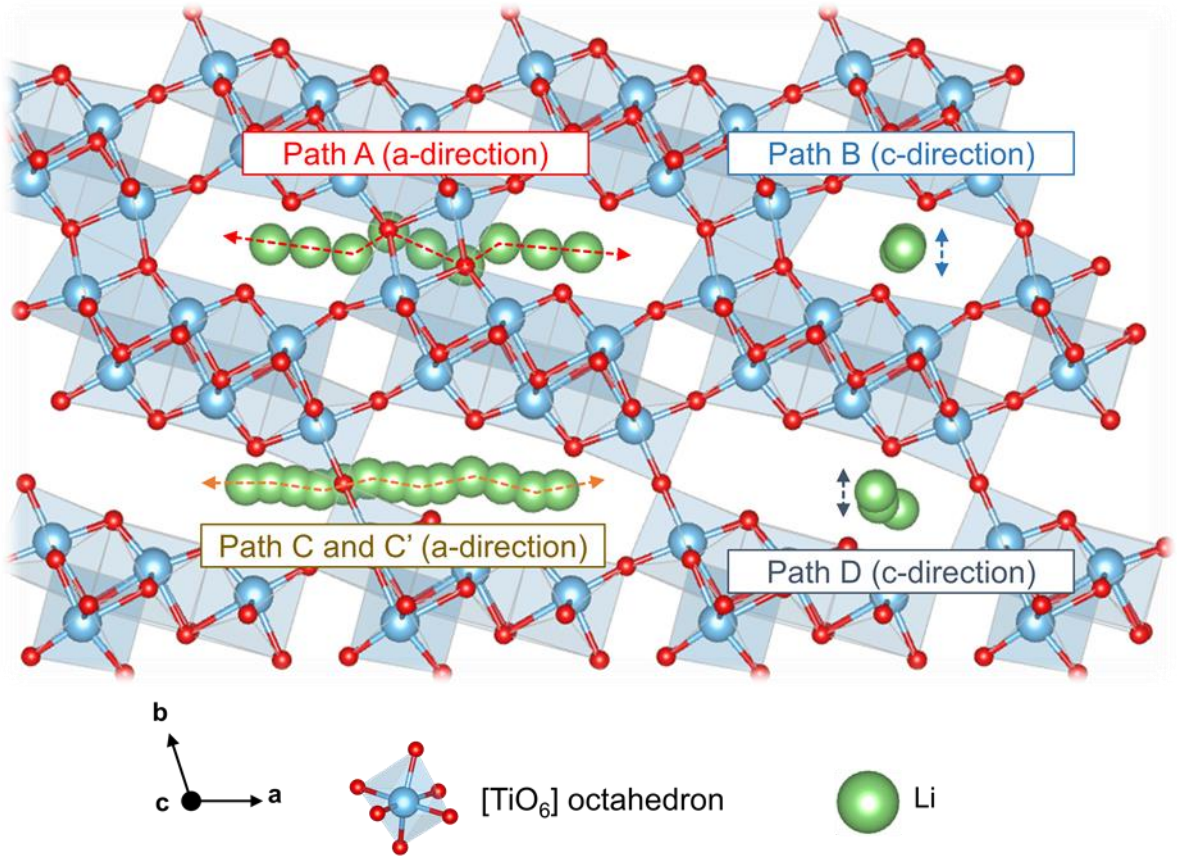

Figure S4. Atomic crystal structure of Li-incorporated $Ti_{12}O_{25}$ and possible pathways for Li migration inside the crystal. The paths A and C represent Li migrations in the a-direction, and the paths B and C correspond to the movements of Li in the c-direction.

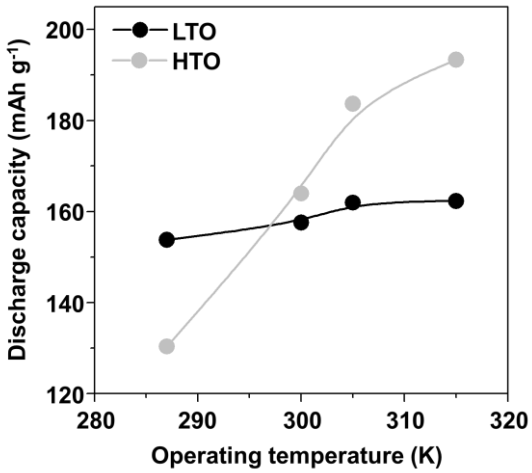

Figure S5. Discharge capacities at various operating temperatures: Comparison between HTO (Li diffusion-controlled process) and $Li_4Ti_5O_{12}$ (electron conduction-controlled process). It is well known that the electrochemical performance of spinel LTO is mainly limited by its intrinsically low electronic conductivity.[S4]

Table S1 Diffusion characteristics of Li inside the HTO crystal.

		Migration distance (d)	Energy barrier (E_{act})	Diffusivity at 305K[a)] (D)
		Å	eV	$cm^2\ s^{-1}$
Path A	a-direction	9.34	1.05	3.82×10^{-19}
Path B	c-direction	2.92	0.157	2.16×10^{-5}
Path C	a-direction	5.82	0.740	2.04×10^{-14}
Path C'	a-direction (inside pore)	3.68	0.637	4.05×10^{-13}
Path D	c-direction	3.98	0.271	5.22×10^{-7}

Note. In DFT calculations, a $Li_{0.5}Ti_{12}O_{25}$ crystal model was used to evaluate the energy barrier.

[a)]Diffusivity was calculated using the Einstein-Smoluchowski relation: $D = g\Gamma d^2$

where $g(\cong 1)$ is a geometric factor, $\Gamma(= \nu^* \exp(-E_{act}/k_B T))$ is a hopping frequency between sites ($\nu^* \cong 10^{13}$) and d is the migration distance.

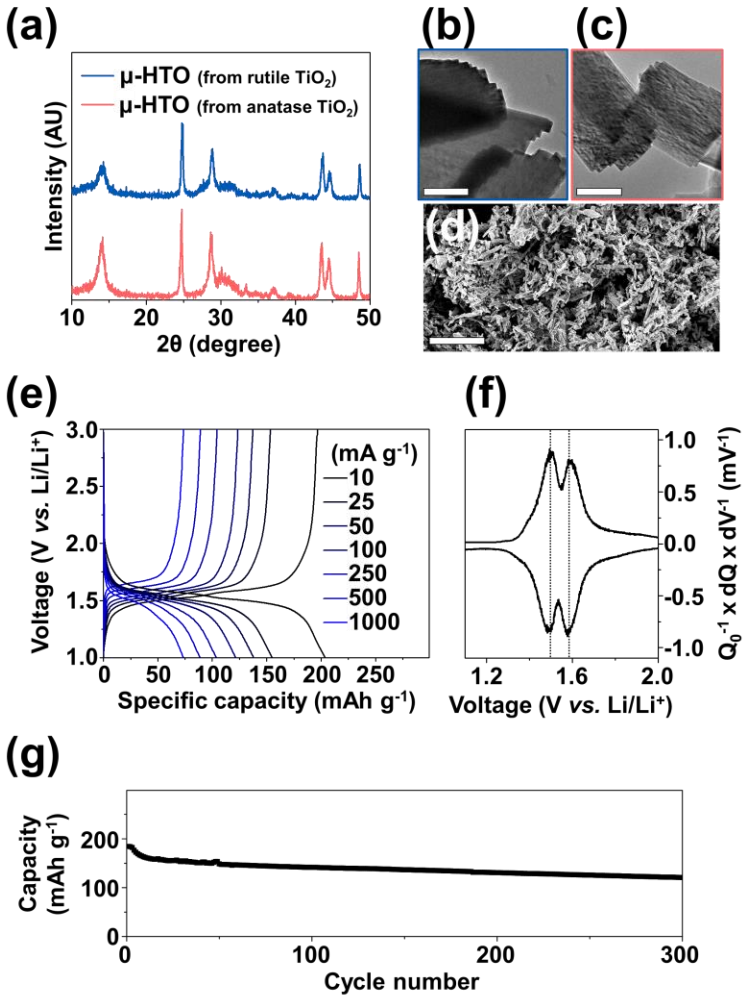

Figure S6. XRD patterns (a) and TEM images of the prepared μ-HTO crystals synthesized using pure rutile (b) and anatase (c) TiO_2 as starting materials. Scale bars correspond to 0.2 μm. (d) SEM image of a synthesized μ-HTO crystal. Scale bar corresponds to 10 μm. (e) Galvanostatic charge/discharge voltage profiles of μ-HTO made from rutile TiO_2 at various current densities from 10 mA g^{-1} to 1,000 mA g^{-1}. (f) Corresponding differential capacities obtained at 10 mA g^{-1}. The profiles clearly show the potential region of the phase transition (at 1.50 V and 1.58 V) during the Li intercalation/deintercalation process, indicative of a two-phase mechanism of lithiation. (g) Discharge capacities of the μ-HTO at 25 mA g^{-1} during the galvanostatic charge/discharge cycles.

Detailed description of the electrochemical performance of μ-HTO

Figure S6 shows characterization and electrochemical data for two kinds of μ-HTO materials synthesized from pure anatase or rutile TiO_2. X-ray diffraction (XRD) patterns of both μ-HTO crystals are in agreement with the previously reported pattern (Figure S6a), which indicates that the HTO particles with a high crystallinity were successfully synthesized.[12,13] Transmission electron microscopy (TEM) images and the scanning electron microscopy (SEM) image in Figure S6b-d reveal that both μ-HTO particles are identical rod-shaped and micrometer-sized particles having transversal lengths of about 0.4 μm and longitudinal lengths of 1~10 μm.

Galvanostatic charge/discharge measurements of the μ-HTO were performed between 1.0 and 3.0 V (*vs.* Li/Li^+) at various rates from 10 mA g^{-1} to 1,000 mA g^{-1}. The electrode composed of μ-HTO was stably charged and discharged with 95~99% Coulombic efficiency, and apparent voltage plateaus were consistently observed (Figure S6e). The electrode delivered reversible capacities of 192, 154, 137, 124, 104, 89, and 74 mAh g^{-1} at current densities of 10, 25, 50, 100, 250, 500, and 1,000 mA g^{-1}, respectively. In corresponding differential capacities (Figure S6f), there are two voltage plateau regions centered at 1.50 V and 1.58 V (*vs.* Li/Li^+). The two separated voltage plateaus suggest two types of Li insertion sites and a subsequent phase transformation.[S1] The μ-HTO showed a capacity retention of 66% during 300 charge/discharge measurements. The predictable reason for the capacity fading during the repetitive cycles is that irreversibly inserted Li obstructs further lithiation at confined areas of bulky μ-HTO crystals.

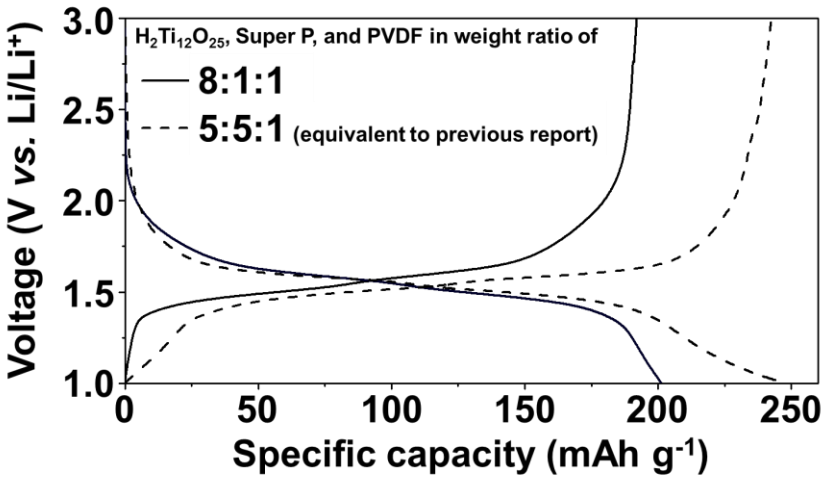

Figure S7. Galvanostatic charge/discharge voltage profiles (obtained at 10 mA g^{-1}) of HTO electrodes with different weight ratios of μ-HTO/conductive carbon (Super P)/binder. In the case of a 5:5:1 ratio, the electrode delivers a discharge capacity of more than 240 mAh g^{-1}, which is in good agreement with the results of previous research.[13] The inordinately high content of the conductive carbon additive significantly reduces the volumetric energy density and cost-effectiveness of the electrode. Therefore, from a practical perspective, we selected a weight ratio of 8:1:1 (HTO:Super P:PVDF) for the electrochemical evaluations of the as-prepared HTO electrodes.

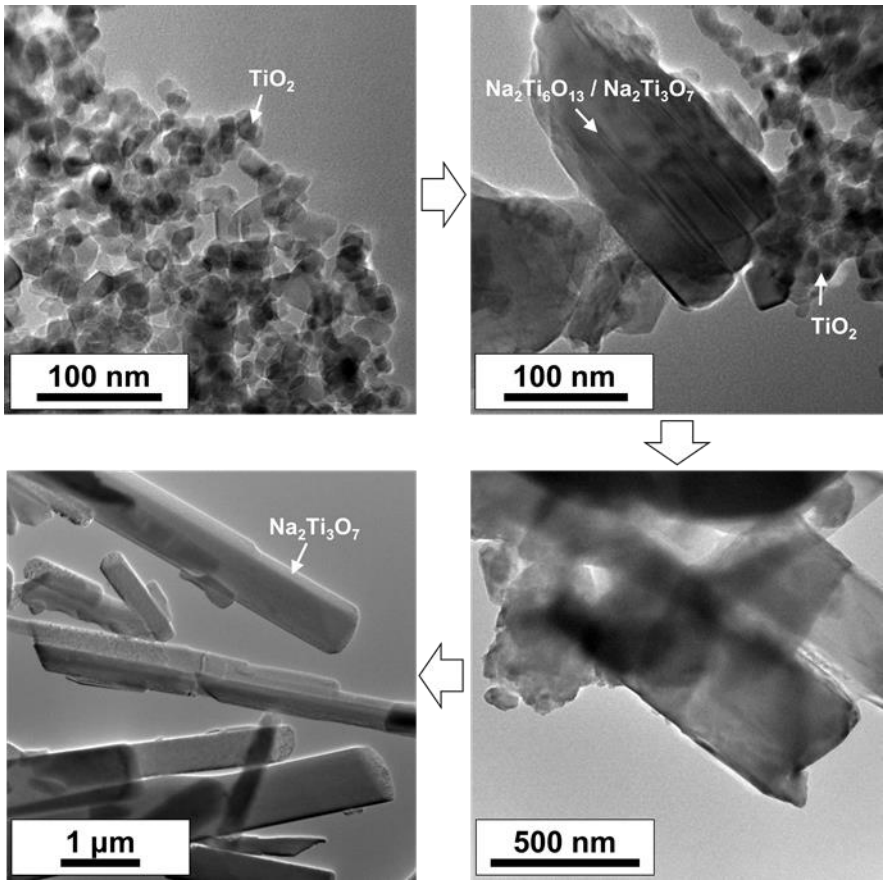

Figure S8. TEM images of samples obtained during the following conversion reaction: $TiO_2+Na_2CO_3 \rightarrow Na_2Ti_3O_6$.

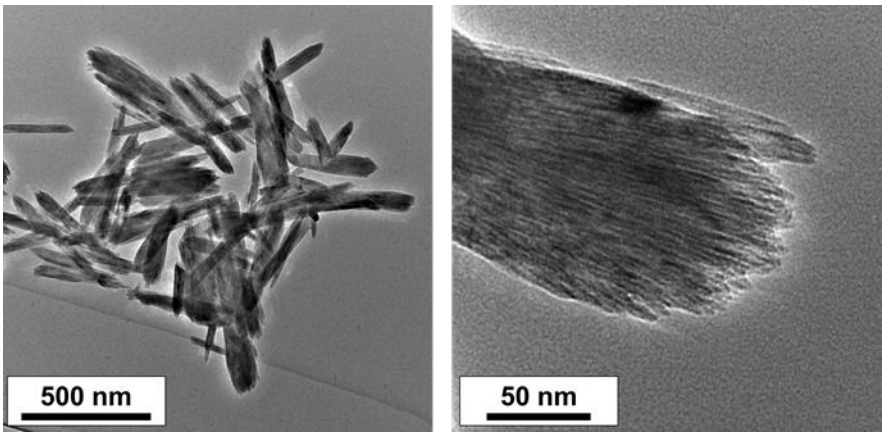

Figure S9. TEM images of nanostructured $H_2Ti_3O_7$ with the shape of a nano-bundle before thermally induced dehydration and condensation reactions at 260 ºC.

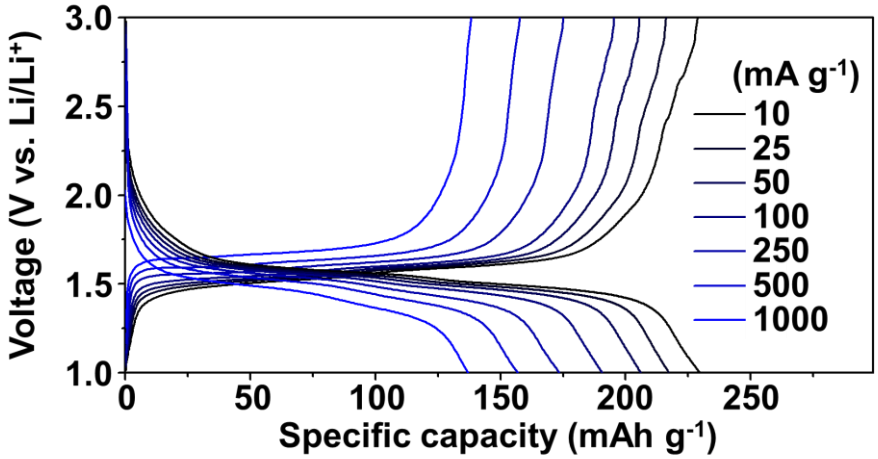

Figure S10. Galvanostatic charge/discharge voltage profiles of n-HTO at various current densities ranging from 10 to 1,000 mA g^{-1}.

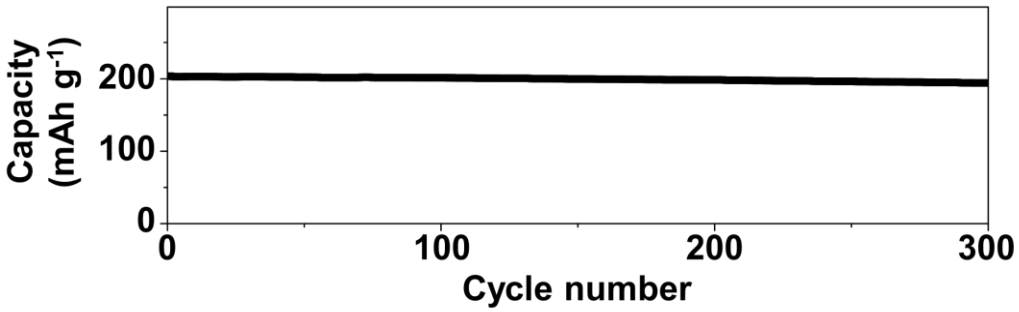

Figure S11. Discharge capacities of n-HTO at 25 mA g^{-1} during the galvanostatic charge/discharge cycles.

REFERENCES

S1 Paolella, A.; Bertoni, G.; Dilena, E.; Marras, S.; Ansaldo, A.; Manna, L.; George, C. Redox Centers Evolution in Phospho-Olivine Type ($LiFe_{0.5}Mn_{0.5}PO_4$) Nanoplatelets with Uniform Cation Distribution. *Nano Lett.* **2014**, *14,* 1477-1483.

S2 Kikkawa, S.; Yasuda, F.; Koizumi, M. Ionic Conductivities of $Na_2Ti_3O_7$, $K_2Ti_4O_9$ and Their Related Materials. *Mat. Res. Bull.* **1985**, *20,* 1221-1227.

S3 Izawa, H.; Kikkawa, S.; Koizumi, M. Ion Exchange and Dehydration of Layered Titanates, $Na_2Ti_3O_7$ and $K_2Ti_4O_9$. *J. Phys. Chem.* **1982**, *86*, 5023-5026.

S4 Zhang, Q.; Li, X. Recent Developments in the Doped-$Li_4Ti_5O_{12}$ Anode Materials of Lithium-Ion Batteries for Improving the Rate Capability. *Int. J. Electrochem. Sci.* **2013**, *8*, 6449-6456.